We have made major and careful modifications to the original manuscript according to all the comments and suggestions from the reviewers. The three major modifications include:

(1) Clarification of the objective of this study

The primary aim of this study is to propose a novel, potential approach to describe the wavelength-dependent aerosol scattering effects using H_2O retrievals, rather than to only retrieve any specific aerosol optical properties as we stated in our first draft, but a series of sensitivity tests to investigate the impacts from aerosol scattering properties on our results have been added in this revised manuscript. This study is an important step towards the direction of fully quantifying the aerosol properties and aerosol scattering effects relevant to greenhouse gas (GHG) retrievals from space. We demonstrated the proposed approach in a complex urban environment in the LA basin using measurements from CLARS and simulations from a 2S-ESS radiative transfer (RT) model. The results from this study show that (1) aerosol scattering effect is the primary contributor to the variations in H_2O SCDs retrieved from multiple bands, and (2) a significant linear correlation is also found between variations in H_2O SCD retrievals from multiple bands and corresponding AOD data; this correlation is associated with asymmetry parameter (g), which is a first-order measure of the aerosol scattering phase function. The conclusion is that, these evidences from both measurements and simulations suggest that wavelength-dependent aerosol scattering effects can be derived using H_2O retrievals from multiple bands. In the revised manuscript (attached in the end), we changed the title and abstract accordingly.

(2) Time range and control experiments in Figure 6

We changed the time range (Figure 3 and 6) to between 9:00 and 15:00 local time to show only the data with solar zenith angles (SZAs) less than 60°, similar to the majority of satellite observations, to exclude the retrievals with large SZAs which may introduce large uncertainty. This time range includes the local overpass times of around 10:00 for SCIAMCHY and around 13:30 for GOSAT, OCO-2, and upcoming TanSat. To explore the role of aerosol scattering in the variations in H_2O SCDs, two new control experiments are shown in Figure 6. In the first control experiment, the AOD data are fixed at the clear-day level, for which the lowest AOD across the year is used, for all hours across the day. In the second control experiment, the AOD is fixed at the aerosol-free level, which is the zero for all hours across the day.

(3) Sensitivity tests on aerosol scattering properties

Figure 7 is added to examine the sensitivity of the correlation, between variations in H_2O SCDs and the corresponding AOP, to aerosol scattering properties, mainly single scattering albedo (SSA) and asymmetry parameter (g), using the 2S-ESS RT model with aerosol compositions from five composite types. Four different control experiments are implemented. The results show that (a) correlation between AOD and extent of variations in H_2O SCDs is robust and significant, and the difference in H_2O abundance and g are responsible for the difference of slopes between the winter-spring and summer-autumn periods; (b) the variations of SSA and g are not the key contributors to the variations of the standard deviations of H_2O SCDs; and (c) g is the main contributor to the ratio of the changes (the slope from linear regression). Moreover, Figure 5 was added to show the monthly-averaged climatological aerosol compositions for the five composite MERRA aerosols in the basin, and Table 1 was added to show the corresponding aerosol single scattering properties for the five composite aerosols.

Please refer to the revised manuscript (attached in the end) for details.

Anonymous Referee #1

Received and published: 20 July 2016

We thank the Reviewer #1 for his/her constructive comments and suggestions to improve the quality and clarity of our manuscript.

Item-by-item responses to the specific comments are provided below, in which the reviews' comments are in **blue**, our responses in **black**, and modifications of the original manuscript are indicated by highlight in **yellow**. The revised manuscript with highlighted changes is attached in the end.

General comments:

The authors describe a potential method that can assist the derivation of aerosol effects of GHG retrievals from space. The method uses measurements and retrievals of water vapor from lines at the SWIR (1250-2500nm), and which shows dependency in water vapor retrievals that are correlated with the amount of aerosols in the atmosphere. The overall idea is innovative and interesting. However, there are some caveats to the method, and some of the assumptions that the method rely on, are not completely supported in the manuscript. The manuscript would benefit from additional sensitivity tests (as described below) and should emphasize or describe more accurately how the suggested method can assist in constraining aerosol optical properties and which optical properties exactly. Overall, it is not entirely clear how the method can assist real-time retrievals, since the method described uses pre-assigned aerosol properties and phase function to get the best fit of the water vapor.

We thank the reviewer for this comment which led us to make substantial revisions to the manuscript. In the revised manuscript, we clarified the aim of this study. It is to propose a novel approach to describe the wavelength-dependent aerosol scattering effects using H_2O retrievals from multiple bands. We also added Figure 7 to examine the sensitivity of the linear correlation between AOD and the variations in H_2O SCDs on SSA and g, two important scattering properties of aerosol. Rather than providing a new method of real-time retrieval of AOD or other optical properties, our proposed approach improves our understanding of aerosol scattering effects on H_2O retrievals, which provides a sensitive way to quantify the effects of aerosol scattering in greenhouse gas retrievals and potentially contribute toward reducing errors of greenhouse gas retrievals from space.

The authors did not discuss how different type and aerosol properties might affect that goodness of fit. It seems that the aerosol amount (i.e., AOD), and not the specific aerosol property are responsible for the trend in the water vapor. Hence, it is not clear how much the method is sensitive or helpful to constrain aerosol optical properties (e.g. size distribution, SSA, refractive index), as stated, or just aerosol relative amount/trends. It would be insightful to see how simulations using different aerosol properties as input, scaled by the AERONET AOD during the day, changes the best fit, as shown in Fig. 5c.

We appreciate these suggestions. As shown in Figure 4, AOD is found to linearly correlated with variations in H_2O SCDs. To examine the sensitivity of the correlation to aerosol scattering properties, mainly SSA and g, we run the 2S-ESS RT model, with AOD inputs from AERONET, daily varying aerosol compositions (five types: organic carbon, black carbon, sulfate, dust, sea salt) from MERRA reanalysis data and single scattering aerosol properties calculated by the GOCART model. The result is shown in Figure 7 in the revised manuscript. From the control experiments, we found that (a) correlation between AOD and

variations in H_2O SCDs is robust and significant, and the difference in H_2O abundance and g are responsible for the difference of slopes between the winter-spring and summer-autumn periods; (b) the variations of SSA and g are not the key contributors to the variations of the standard deviations of H_2O SCDs; and (c) g is the main contributor to the ratio of AOD changes to variations in the retrieved H_2O SCD. For more detail, please see Section 5.2 in the revised manuscript.

Also, the authors state that their analysis is based on water vapor absorption alone in the wavelength range of investigation. However, CO2, CH4 and N2O absorb as well in this wavelength range and the authors should mention how the combined absorption of those gases might affect the suggested method in terms of the IC, and the ability to de-convolve the aerosol trend from the GHG mixture, given their variability during the day.

Thank you for this comment, pointing out that clarification was needed. Absorptions by other gas molecules have been considered in the 2S-ESS RT model used. In the model, absorptions by the dominant gas molecules in the atmosphere, including H_2O, CO_2, N_2O, CO, CH_4, O_2, N_2 and HDO, are considered by using an *a priori* atmospheric profile obtained from the National Centers for Environmental Prediction (NCEP)-National Center for Atmospheric Research (NCAR) reanalysis data (Kalnay et al., 1996). We added the above statements to Section 3 in the revised manuscript.

In the chosen 15 H_2O absorption bands, H_2O absorption is dominant. The ratio of absorption by water vapor to the all gases for the 15 bands is greater than 90% on average. Given the dominant absorption of H_2O in these bands, full consideration of the absorption by other gases, and the high IC of retrieving H_2O SCDs, we believe that the retrievals of H_2O SCDs from the 15 bands should be accurate and the impact from other gases on the relation between AOD and variation in H_2O should be negligible.

Given a situation where aerosol amount/properties are unknown (i.e. real retrieval), what would be the uncertainty level of the retrieved water vapor amount and aerosol (properties or AOD?).

Thank you for this question. As shown in Figure 7 of the revised manuscript, the variations in H_2O SCDs are robustly and linearly correlated with AOD, and the rate of change is related to the asymmetry parameter of aerosol scattering. The coefficient of determination from linear regression can be used to indicate the uncertainty level. From the CLARS measurements, the AOD variability can explain about 50% of the variations of scattering effects on H_2O retrievals (Figure 4), while based on the model simulations from the 2S-ESS model, AOD variability can explain about 76-80% (Figure 7(a)).

The authors are showing results from wavelengths in the range of 1250-2500 nm, while the AERONET instrument measure only up to 1020 nm. The authors state that they use an extrapolated angstrom exponent to derive the aerosol wavelength dependency to use in the model, however, at the FTS wavelength range, there is already very little dependence, as already between 870 and 1020 nm bands there is very little dependence (Fig. d, both panels). Hence, it is unclear how the method can constrain the aerosol properties since in this wavelength range the wavelength dependency is very weak.

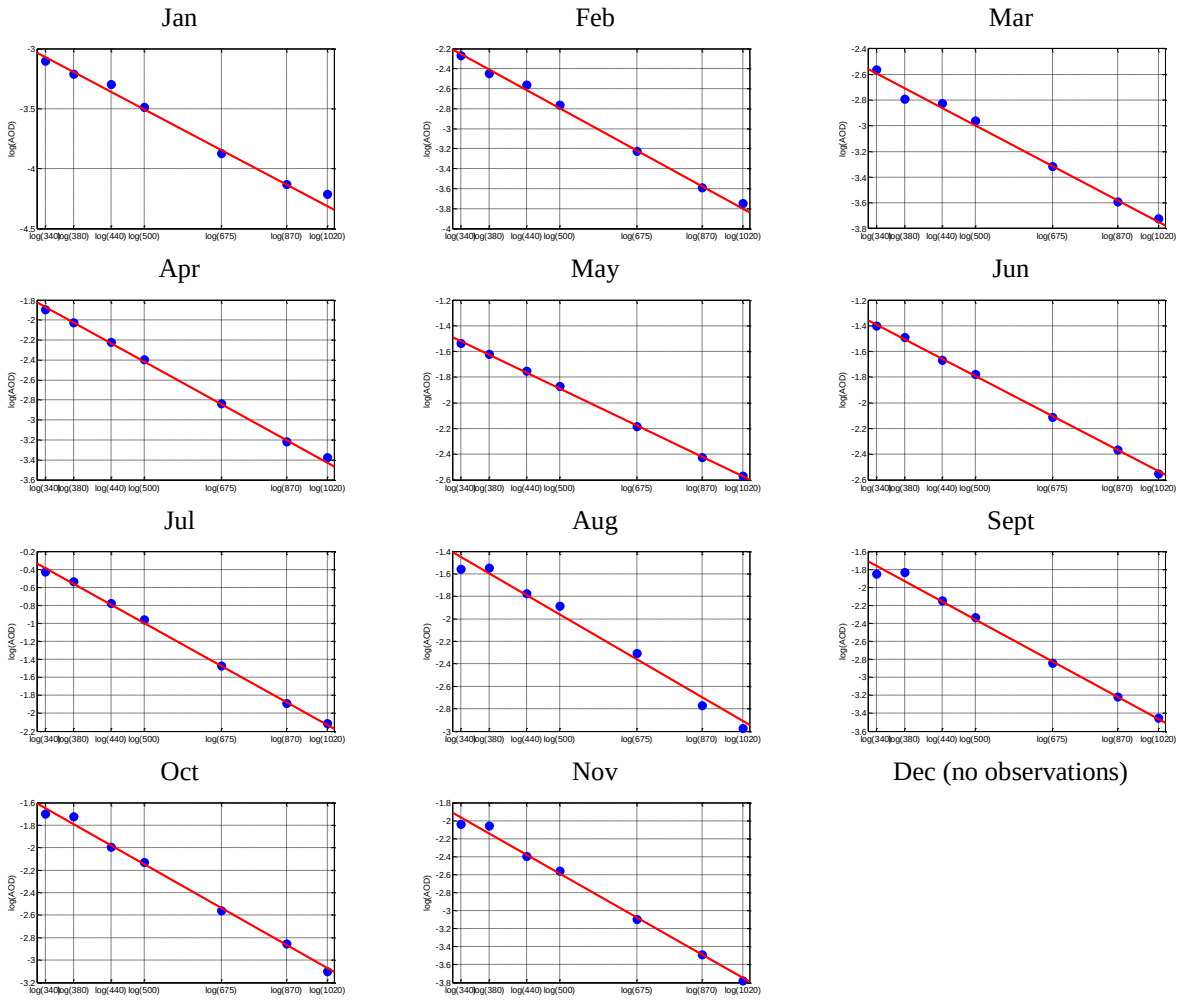

Figure I. examples from applying linear regressions using the logarithmic form of Ångström exponent law on the AERONET AOD data at noon time around 13:00, for the 11 different months, selected from the 68 days of data shown in Figure 4 and 7. The blue dots are the AERONET AOD measurements in the seven different bands (340nm, 380nm, 440nm, 500nm, 870nm and 1020nm) and the red line is linear regression result from the first 6 of the 7 bands (that is, 1020nm is excluded). Therefore, the closeness of the AOD at 1020nm to the fitted red line indicates the strength of the wavelength dependence that follows the exponential law. The averaged bias between the AOD and the red line value at 1020nm for all the 68 days is 9.82±10.02% (mean and one standard deviation).

Thank you for this comment. To examine the wavelength dependence of all the data used, especially on the near-infrared band at 1020nm, we checked the AERONET AOD data that were used in Figure 4 and Figure 7 with 68 days of data. The dependence can be described by the following Ångström exponent law:

$$\frac{\tau}{\tau_0} = \left(\frac{\lambda}{\lambda_0}\right)^{-k} \quad \boldsymbol{OR} \quad \log(\tau) = -k * \log(\lambda) + c \;\; [c \; is \; a \; constant]$$

Where λ and τ are the wavelength and the corresponding AERONET AOD, and λ_0 and τ_0 are the reference wavelength and the corresponding AOD, and k is the Ångström exponent. If the AOD measurements in different wavelengths follow this exponent law, we would expect the AOD has strong wavelength dependence. Figure I shows examples from applying linear regressions using the logarithmic form of Ångström exponent law on the AERONET AOD data at noon time around 13:00, for the 11 different months, selected from the 68 days of data shown in Figure 4 and 7. The blue dots are the AERONET AOD

measurements in the seven different bands (340nm, 380nm, 440nm, 500nm, 870nm and 1020nm) and the red line is linear regression result from the first 6 of the 7 bands (that is, 1020nm is excluded). Therefore, the closeness of the AOD at 1020nm to the fitted red line indicates the strength of the wavelength dependence that follows the exponential law. We can see, in general, the wavelength dependence follows the exponent law, suggesting the dependence is strong. We further calculated the averaged bias between the AOD and the red line value at 1020nm. The average bias for all the 68 days is 9.82±10.02% (mean and one standard deviation), which is small. Therefore, we conclude that the wavelength dependences for most of the 68 days are strong. We added Figure I in the supplementary material.

What is the IC available for constraining aerosol properties?

Thank you for this question. In this study, we used the IC value to evaluate the efficiency of band channels selected for retrieval and assess the precision of H_2O retrieval in the selected 15 bands. However, it is hard to relate the IC values with the correlation between AOD (or other aerosol scattering properties) and variations in H_2O SCDs. Instead, we used the R^2 quantify the uncertainty of the correlation between them, and control experiments using 2S-ESS to examine its sensitivity to aerosol scattering properties. From the CLARS measurements, the AOD variability can explain about 50% of the variations of scattering effects on H_2O retrievals (Figure 4), while based on the model simulations from the 2S-ESS model, AOD variability can explain about 76-80% (Figure 7(a)). The results from sensitivity test is presented in Section 5.2 in the revised manuscript.

Again, it seems that the method can give the general aerosol amount, but cannot differentiate between different aerosol types, which have different optical properties.

Thank you for this comment. We agree that we do not differentiate between different aerosol types. One of the key conclusions from this study is that AOD (from all aerosol types) is linearly and significantly correlated with variations in H2O SCDs, and that the asymmetric parameter, relevant to aerosol scattering phase, is responsible for the rate of changes between them. However, we cannot differentiate between different aerosol types. But in the revised manuscript, we added Figure 7 to examine the sensitivity of this linear correlation on SSA and g, two important scattering properties of aerosol that are influenced by the aerosol compositions (five composition types from MERRA were used: organic carbon, black carbon, sulfate, dust and sea salt) and their different scattering properties. Please refer to Section 5.2 in the revised manuscript for details.

Also, from Fig. 4, it is interesting to note that the aerosol wavelength dependency is changing during the course of the day. Did the authors explored how this local behavior might affect the suggested method?

Thank you for this comment. The changing wavelength dependency of AOD can be inferred from the changing Ångström parameter during the day, as shown in the following figure II, and this change of Ångström parameter results from the change of aerosol compositions. In Figure 7 of the revised manuscript, we show results of four controlled sensitivity tests using the aerosol compositions from MERRA reanalysis data for five composite types (organic carbon, black carbon, sulfate, dust, sea salt) using the 2S-ESS model. The results show that the effective asymmetry parameter of aerosol scattering, as a composition-weighted sum, has impact on the correlation slope between AOD and the magnitude of the variations in H_2O SCDs. Please refer to Section 5.2 in the revised manuscript for more details.

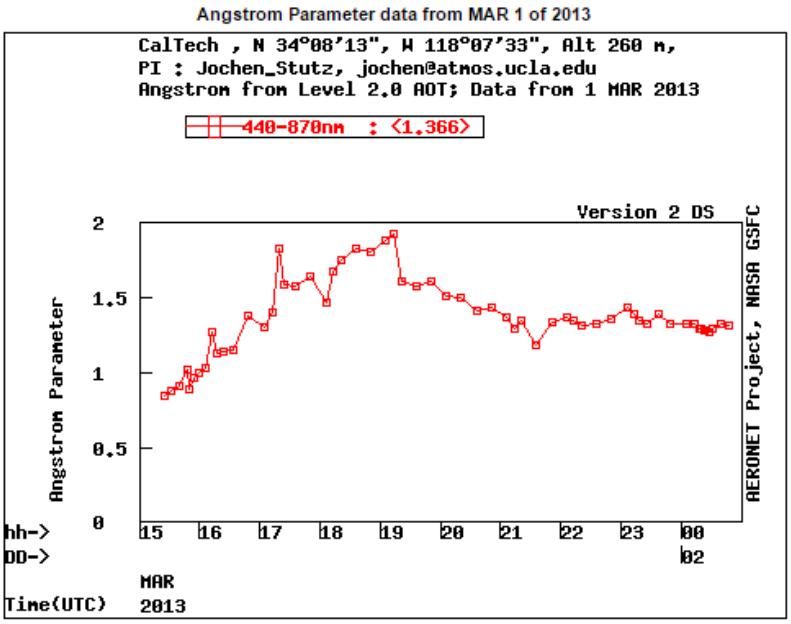

Figure II. Angstrom parameter from AEROENT-Caltech on March 01, 2013. This figure was downloaded from http://aeronet.gsfc.nasa.gov/.

Some additional questions, and points to note:

1. Small aerosol, such as urban pollution and Biomass burning are not expected to have such a large scattering effect at the FTS wavelength range. Please expand the discussion on this and on the ability of the method to be helpful under events that are dominated by these type of aerosols, rather than dust for example.

Thank you for this good suggestion. Figure 5 was added in the revised manuscript to show the monthly averaged aerosol compositions (five composition types from MERRA: organic carbon, black carbon, sulfate, dust and sea salt) in 2013 in the LA basin, and their corresponding aerosol scattering properties are also shown in Table 1. We can see that, in general, sea salt dominates in the summer-autumn period while dust dominates in the winter-spring period. For small aerosols, such as black carbon, organic carbon and sulfate, their ratios are relatively small but changes during the year with larger proportion in summer than in winter. From Table 1 we can see that the SSA and g of these small aerosols are much smaller than that of dust and sea salt. Therefore, under the events that dominate by these types of small aerosols, the effective g will become smaller and therefore the rate of change (the slope from linear regression) will become smaller, according to the results from control experiments shown in Figure 7(e). We added these statements in the Section 5.2 of the revised manuscript.

2. The authors are stating that the method can assist in constraining aerosol optical properties, but the majority of the discussion is around AOD, which is not an internal property of the aerosol. Please try to define the objectives and discussion in a more accurate way.

Thank you for this good comment which led us to make substantial revisions to the manuscript. In the revised manuscript, we clarified the aim of this study. It is to propose a novel approach to describe the wavelength-dependent aerosol scattering effects using H_2O retrievals from multiple bands. We also added Figure 7 to examine the sensitivity of the linear correlation between AOD and the variations in H_2O SCDs

on SSA and g, two important scattering properties of aerosol. We also changed the title and abstract accordingly.

3. Please provide an explanation of the GHG retrievals, especially on the spectral range of interest and whether these are overlapping with the wavelength range of the water vapor measurements. How these would interfere with each other in an end-to-end retrieval scheme?

The 15 bands we chosen to retrieve H_2O lie in the range of 4000 to 8000 cm^{-1}. The GHGs, such as CO_2 and CH_4, are retrieved from current satellite missions using GHGs absorption bands in around 6200 cm^{-1} (weak CO_2 absorption band) and 4850 cm^{-1} (strong CO_2 absorption band) for CO_2 and 6000 cm^{-1} for CH_4.

In our study, the 15 H_2O bands are dominated by H_2O absorptions. Apart from H_2O, in the 2S-ESS model, absorptions by other gas molecules in the atmosphere, including CO_2, N_2O, CO, CH_4, O_2, N_2 and HDO, are considered by using an *a priori* atmospheric profile obtained from NCEP-NCAR reanalysis data. Even though in this study, we assume that only one state variable, i.e., H_2O SCD, is retrieved. But from the IC results shown in Figure 2, we can see that the average IC is high (about 6 on average) and similar among all bands, which indicates that our retrieved H_2O SCD has very high retrieval precision compared with the *a priori* information.

Retrieval of GHGs from satellite usually retrieves the GHGs and H_2O simultaneously to account for the impact from H_2O absorption, which is nonnegligible in the CO_2 or CH_4 absorption bands.

Minor comments:

Fig. 3, please add label on the x-axis

Done.

Page 6, lines 13-15, it is not clear whether the RT simulations are being done for 5 aerosol type or a combination of those 5 to give a mixture aerosol type that should represent the LA basin aerosols.

In this study, the RT simulations were done for a combination of the five composite aerosol types in the LA basin. Using the compositions of the five composite MERRA aerosols and their scattering properties, the effective SSA and g of aerosol scattering are calculated, respectively, as the composition-weighted sum for all types, and then incorporated into the 2S-ESS RT model. We added the above statements to Section 5 in the revised manuscript.

The following documents are the revised manuscript (with changes highlighted) and the supplementary figure:

Aerosol Scattering Effects on Water Vapor Retrievals over the Los Angeles Basin

Zhao-Cheng Zeng[1,2], Qiong Zhang[1], Vijay Natraj[3], Jack S. Margolis[4], Run-Lie Shia[1], Sally Newman[1], Dejian Fu[3], Thomas J. Pongetti[3], Kam W. Wong[1,3], Stanley P. Sander[3], Paul O. Wennberg[1] and Yuk L. Yung[1]

[1]Division of Geological and Planetary Sciences, California Institute of Technology, Pasadena, CA 91125, USA
[2]Institute of Space and Earth Information Science, The Chinese University of Hong Kong, Hong Kong, China
[3]Jet Propulsion Laboratory, California Institute of Technology, Pasadena, CA 91109, USA
[4]1842 Rose Villa St., Pasadena, CA 91107, USA

Correspondence to: Zhao-Cheng Zeng (zcz@gps.caltech.edu)

Abstract. In this study, we propose a novel approach to describe the scattering effects of atmospheric aerosols in a complex urban environment using water vapor (H_2O) slant column measurements in the near infrared. This approach is demonstrated using measurements from the California Laboratory for Atmospheric Remote Sensing Fourier Transform Spectrometer on the top of Mt. Wilson, California, and a two-stream-exact single scattering radiative transfer (RT) model. From the spectral measurements, we retrieve H_2O slant column density (SCD) using 15 different absorption bands between 4000 and 8000 cm^{-1}. Due to the wavelength dependence of aerosol scattering, large variations in H_2O SCD retrievals are observed as a function of wavelength. Moreover, the variations are found to be correlated with aerosol optical depths (AOD) measured at the AERONET-Caltech station. Simulation results from the RT model reproduce this correlation and show that the aerosol scattering effect is the primary contributor to the variations in the wavelength dependence of the H_2O SCD retrievals. A significant linear correlation is also found between variations in H_2O SCD retrievals from different bands and corresponding AOD data; this correlation is associated with the asymmetry parameter, which is a first-order measure of the aerosol scattering phase function. The evidence from both measurements and simulations suggests that wavelength-dependent aerosol scattering effects can be derived using H_2O retrievals from multiple bands. The understanding of aerosol scattering effects on H_2O retrievals provides a sensitive way to quantify the effect of aerosol scattering on greenhouse gas retrievals and could potentially contribute towards reducing biases in greenhouse gas retrievals from space.

1 Introduction

Greenhouse gas (GHG) observations from space provide unprecedented global measurements of column GHG concentration, facilitating inference of carbon fluxes on regional scales (Yoshida et al., 2011; Crisp et al., 2012). However, atmospheric aerosol scattering has been shown to have a considerable impact on the retrieval of GHGs from space-based observations in the near infrared (Aben et al., 2007; Yoshida et al., 2011; O'Dell et al., 2012). A study by O'Dell et al. (2012) showed that

the error budget in the satellite retrievals of column-averaged dry-air mole fraction of CO_2 (XCO_2) is dominated by systematic errors due to imperfect characterization of cloud and aerosol properties. Previous studies also showed that the bias can be greatly mitigated by incorporating simple aerosol properties into the retrieval state variables (Butz et al., 2009; Guerlet et al., 2013). It is therefore crucial to characterize the aerosol properties for the GHG retrieval algorithm. However, aerosols have complex types and size distributions and are highly variable in number density. Their optical properties are very hard to measure directly (Seinfeld and Pandis, 2006). The global ground-based aerosol monitoring network, AERONET (Holben et al., 1998), has been providing high-accuracy measurements of total aerosol optical depth (AOD) from the ultraviolet to the near infrared, but is sparsely distributed, suggesting that it would be useful to have further means of constraining aerosol optical properties.

Water vapor (H_2O) has absorption features across the electromagnetic spectrum, from the ultraviolet to the infrared. In a non-scattering atmosphere, H_2O retrievals from different absorption bands would give exactly the same value. However, due to the wavelength-dependent aerosol scattering (Eck et al., 1999; Zhang et al., 2015), the different light path changes in different absorption bands result in discrepancies in H_2O retrievals. This variation in H_2O retrievals from different bands can therefore provide information on aerosol properties. Based on this theory, we propose a novel approach to describe the aerosol scattering effects using the variation in H_2O retrievals from multiple bands. This approach is illustrated with data from The California Laboratory for Atmospheric Remote Sensing (CLARS), which continuously collects high-resolution spectra in the near infrared. A two-stream-exact single scattering (2S-ESS) radiative transfer (RT) model is used to simulate the observations and explain the physical mechanism behind the proposed approach. The additional information on aerosol optical properties gained by applying this approach could be used to improve retrievals of GHGs from space in the presence of aerosols.

In Section 2, a detailed description of the CLARS-FTS is presented. Section 3 introduces the 15 different bands chosen for retrieving H_2O from CLARS measurements. In Section 4, the correlation between variations in H_2O retrievals from different bands and corresponding AOD data from AERONET-Caltech is discussed. In Section 5, the role of aerosol scattering on the variations in H_2O retrievals is illustrated using the 2S-ESS RT model. Discussion and conclusions are presented in Sections 6 and 7, respectively.

2 CLARS

The CLARS-FTS is located near the top of Mt. Wilson at an altitude of 1670 m a.s.l. overlooking 28 land target sites in Los Angeles (Supplemental material Table 1 and Figure 1 of Fu et al., 2014; Wong et al., 2015; Wong et al., 2016). It offers continuous high-resolution spectral measurements from 4000 to 8000 cm^{-1}. As shown in Figure 1, CLARS-FTS has two operating modes: the Spectralon Viewing Observation (SVO) mode and the Los Angeles Basin Surveys (LABS) mode. In SVO mode, the FTS looks at a Spectralon® plate adjacent to the FTS to observe the reflected solar spectrum from the free

troposphere above Mt. Wilson, which is usually above the planetary boundary layer (PBL) and relatively immune to aerosol scattering. In LABS, the FTS looks down at target sites in the LA basin to observe the reflected sunlight, which travels through a long light path within the urban PBL (Figure 1) and undergoes absorption and scattering by gas molecules and aerosols. This observation geometry by LABS mode makes CLARS-FTS measurements not only highly sensitive to the atmospheric composition in the PBL but also very susceptible to influence by aerosol scattering and absorption. This CLARS measurement technique from Mt. Wilson mimics geostationary satellite observations of reflected sunlight and measures atmospheric absorptions by GHGs along the optical paths, including the incident path from the sun to the surface and the reflection path from the surface to the instrument (Xi et al., 2015).

Slant column density (SCD), the total number of absorbing molecules per unit area along the optical path, is retrieved for H_2O using the version 1.0 operational retrieval algorithm of CLARS-FTS (Fu et al., 2014), developed based on the Gas Fitting tool (GFIT) algorithm that has been widely used for the Total Carbon Column Observing Network (TCCON) network (Toon et al., 1992; Wunch et al., 2011). Surface reflection is included in the modified version but aerosol scattering is not taken into account. Thus, errors in the SCD retrieval are largely due to light path changes caused by aerosol scattering, and can be used as a proxy for aerosol loading. A detailed description of the observation system of CLARS-FTS, measurement sequence, operational retrieval algorithms and characteristics of operational data products can be found in Fu et al. (2014). The 15 different bands used in this study for retrieving H_2O SCDs from CLARS-FTS are introduced in Section 3.

3 Bands for H_2O retrievals

H_2O has absorption features across the electromagnetic spectrum including many absorption lines in the near infrared as well as significant continuum absorption. Within the spectral range of CLARS-FTS observations, we carefully select 15 spectral intervals containing dominant H_2O absorption lines, as shown in Figure 2, across the spectral range from 4000 to 8000 cm^{-1} for retrieving H_2O SCD. Each interval is 5 to 14 cm^{-1} wide and contains two to nine moderately strong absorption lines. Rodgers (2000) showed that information analysis is a powerful tool for evaluating the efficiency of band channels selected for retrieval. Therefore, we conduct information analysis by calculating the information content (IC) for each band selected for retrieving H_2O SCD. A detailed theoretical description of the information analysis can be found in Su et al. (2015). The RT model used here is the numerically efficient 2S-ESS RT model (Spurr and Natraj, 2011). The detailed settings for the 2S-ESS model are described in Section 5. In the RT model, absorptions by the dominant gas molecules in the atmosphere, including H_2O, CO_2, N_2O, CO, CH_4, O_2, N_2 and HDO, are considered by using an *a priori* atmospheric profile obtained from the National Center for Environmental Prediction (NCEP)-National Center for Atmospheric Research (NCAR) reanalysis data (Kalnay et al., 1996). Here, we assume that only one state variable, i.e., H_2O SCD, is retrieved. Therefore, the IC values shown in Figure 2 are for H_2O retrieval only; they are indicators of the precision of H_2O retrieval in the selected bands. For

any band with IC value equal to *x*, as many as e^x different atmospheric H_2O states can be distinguished (Rodgers, 2000). The purpose of the IC calculation is to show the sensitivity of each absorption band to the variation of H_2O SCD. While fitting the CLARS-FTS measured spectra, we retrieve more state variables including other trace gas abundances and continuum shape parameters (Fu et al., 2014). From the IC results shown in Figure 2, we can see that the average IC is high (about 6 on average) and similar among all bands, which indicates very high retrieval precision compared with the *a priori* information (Rogers, 2000). H_2O SCDs retrieved from these 15 bands will be shown in the following section.

4 H_2O SCD retrievals from CLARS and its correlation with aerosol optical depth

4.1 Daily variation

Figure 3 shows examples of daily CLARS H_2O SCD retrievals on March 01, 2013 and September 28, 2013. On these two days, there were dense observations for the West Pasadena target retrieved using the 15 bands shown in Figure 2. Observations between 9:00 and 15:00 local time are shown, when the solar zenith angles (SZAs) are less than 60°, similar to the majority of satellite observations. This time period also includes the local overpass times at around 10:00 for SCIAMCHY (Bovensmann et al., 1999) and around 13:30 for GOSAT, OCO-2 and TanSat (Liu et al., 2011). In particular, we compare retrievals from SVO (Figure 3(a)), which is above the PBL (Newman et al., 2013) and therefore relatively unaffected by aerosol scattering, with those from the West Pasadena target (Figure 3(b)), a location in the Los Angeles basin that is influenced by aerosol scattering. The H_2O SCD retrievals from SVO are nearly identical across different wavelengths, and the small differences may be attributed to the band-to-band inconsistency of line parameters. However, H_2O SCD retrievals for West Pasadena show significantly larger variation across different wavelengths. These retrieval differences are much larger than can be attributed to spectroscopic uncertainties alone, and reflect the wavelength dependence of aerosol scattering in the boundary layer. To quantify the variation in the H_2O SCD retrievals from the 15 bands, the standard deviation (σ) of the retrievals is calculated by,

$$\sigma = \sqrt{\sum_{i=1}^{n}[(s_i - \bar{s})^2]/(n-1)}, \quad (1)$$

where n=15 is the number of bands, s_i is the SCD retrieval for band i, and $\bar{s} = (\sum_{i=1}^{n} s_i)/n$ is the mean. The standard deviations in Figure 3 (c) show that the variations in H_2O SCD retrievals monotonically increase throughout the day. As shown in Figure 3 (d), the AOD data on these two days from AERONET-Caltech shows a typical pattern for the LA basin. AOD increases from the morning to the afternoon. Note here that the AERONET station measures mainly in the visible and near-infrared wavelengths from 340 to 1020 nm. However, we assume that they are also good proxies for AOD at longer wavelengths in the near infrared. The increasing trend of AOD corresponds well to that of the standard deviations of H_2O SCD retrievals. This correlation from daily measurements shows the potential of constraining the AOD using the standard deviation of H_2O SCD retrievals. However, apart from aerosol scattering, the daily variation of standard deviations of H_2O

SCD retrievals can also be influenced by differences in observation geometry, such as SZA and relative azimuth angle (AZA), and variations in planetary boundary layer height (PBLH). All of these parameters are changing during the day.

4.2 Seasonal variation

To quantitatively compare the variations in H_2O SCD retrievals and AOD, we choose the daily mean of the data between 12:00 and 14:00 local time when there is generally less haze or fog. This time is also coincident with the local crossing time of the two currently operating GHG observation satellites, GOSAT (Yoshida et al., 2011) and OCO-2 (Crisp et al., 2012). We focus on a two hour period to limit the effect of other parameters on the H_2O retrieval standard deviation, such as solar geometry and PBLH. The closest AERONET AOD data are used as the concurrent AOD data for the CLARS retrievals. If the measurement time difference is more than 30 min, then the CLARS data are not used. AERONET-Caltech has AOD measurements in seven wavelengths from 340 to 1020 nm, and we choose the data at 1020 nm, which is the closest to the wavelengths for retrieving H_2O in this study. Furthermore, the AOD data are scaled to the optical depths along the slant path, which is the aerosol optical path (AOP), according to the SZA and viewing zenith angle of CLARS at West Pasadena (83.1°). Following this procedure, 68 daily mean data pairs are available in 2013 after excluding days (1) that are cloudy according to the images from the visible camera looking at the target and (2) in which there are fewer than three valid observations. We separate the data into two different time periods, the winter-spring season (December to May) and the summer-autumn season (June to November) by considering the different dominant wind directions between winter and summer in Pasadena (Conil and Hall, 2006; Newman et al. 2016). In the summer, the prevailing winds come from the southwest across the basin; in the winter, the winds come from the northeast across the mountains and deserts. Different wind patterns (Newman et al., 2013) suggest that the dominant aerosol types during these two time periods may be different. For each of these two time periods, we expect the CLARS observation geometry and PBLH at noon time to be similar across the days, and therefore assume their effects on H_2O retrievals to be similar. In fact, it will be clear from the RT model simulation in Section 5 that the contributions to the variation in H_2O retrievals from other factors are actually much smaller than those from aerosol scattering, even though the geometry and PBLH change a lot during a day.

Figure 4 shows significant linear correlations between the AOP value and the standard deviation of H_2O SCDs for the two time periods, both with R^2 around 0.5. However, the slopes from linear regression between the AOP and the standard deviation of H_2O SCD retrievals are different. In summer-autumn, the regression slope, an indication of the degree of light path change due to aerosol scattering relative to the change in aerosol loading, is about one half of that in winter-spring, indicating that for the same AOD, the variation in H_2O SCD retrievals in summer-autumn is about twice that in winter-spring. H_2O abundance shows significant seasonal variation in the LA basin, and previous studies have shown, for example, that aerosol optical properties change dramatically with relative humidity (e.g. Thompson et al., 2012). In fact, results from control experiments using the RT model, shown in Section 5, show that the difference in H_2O abundance and aerosol phase

function, indicated by the asymmetry parameter, are responsible for the difference in slope between the winter-spring and summer-autumn periods.

5 Simulations using 2S-ESS RT model

In this section, we use the numerically efficient 2S-ESS RT model (Spurr and Natraj, 2011) to simulate the measurements and quantify the role of aerosol scattering in the variation in H_2O SCDs retrieved from CLARS. The 2S-ESS model performs an exact computation of the single scattering using all moments of the phase function, while the multiply-scattered radiation is calculated using the two-stream approximation. This model has been used for GHG remote sensing in several previous studies (Xi et al., 2015; Zhang et al., 2015; Zhang et al., 2016).

We simulate the spectral radiance observed by CLARS-FTS for the West Pasadena target. The settings for this model are largely the same as those used by Zhang et al. (2015). Some essential settings and modifications are as follows. In this RT model, (1) the *a priori* atmospheric profile is obtained from NCEP-NCAR reanalysis data (Kalnay et al., 1996). The profile has 70 layers from the surface up to 70 km; (2) absorption coefficients for all absorbing gas molecules are derived from the HITRAN version 2008 database (Rothman et al., 2009); (3) the optical depth for each layer is calculated using the Reference Forward Model (Dudhia et al., 2002); (4) the surface reflection is assumed to be Lambertian with a surface albedo of 0.23, measured by Fu et al. (2014) for West Pasadena; (5) Rayleigh scattering by air molecules is considered in this RT model; (6) the observation geometry, including the viewing zenith angle for the West Pasadena target, the daily SZA, and AZA on March 01, 2013 are included in the model; (7) the aerosol scattering phase function in the model is assumed to follow the Henyey-Greenstein type phase function (Henyey and Greenstein, 1941). Climatological aerosol compositions, as percentages of total optical depth, for five types of aerosol (black carbon, organic carbon, sulfate, dust, and sea salt) are obtained from the Modern Era Retrospective analysis for Research and Applications (MERRA) aerosol reanalysis database (Rienecker et al., 2011; Buchard et al., 2015). A more detailed description of the data can be found in Connor et al. (2016). The aerosol single scattering properties, including single scattering albedo (SSA) and asymmetry parameter (g), were computed using the GOCART model (Colarco et al., 2010, Chin et al., 2002). These properties were tabulated for black carbon, organic carbon, sulfate, dust, and sea salt aerosol types, with hygroscopic effects included where appropriate. The averaged values of the scattering parameters are shown in Table 1. Using the compositions of the five composite MERRA aerosols and their scattering properties, the effective SSA and g of aerosol scattering are calculated, respectively, as the composition-weighted sum, and then incorporated into the 2S-ESS RT model. Figure 5 shows the monthly-averaged climatological aerosol compositions for the five composite MERRA aerosols. We can see that, in general, sea salt dominates in the summer-autumn period while dust dominates in the winter-spring period; (8) unlike Zhang et al. (2015), in this study, the average hourly PBLH data measured over late spring in 2010 in LA (Newman et al., 2013) are used. Unlike CO_2, the H_2O mixing ratio varies dramatically with altitude in the atmospheric column (Seinfeld and Pandis, 2006). In the LA basin, a large portion of

H_2O is concentrated within the PBL. Therefore, the PBLH is an important parameter in modeling the effect of scattering on the H_2O retrieval. The model output radiance is convolved using the CLARS-FTS instrument line shape with full width at half maximum (FWHM) = 0.022cm^{-1} (Fu et al., 2014). The spectral resolution is set to be 0.06 cm^{-1}, and the corresponding instrument maximum optical path difference is 5.0 cm. The signal-to-noise ratio is assumed to be constant at 300. We perturb the simulated spectra with Gaussian white noise.

The wavelength range covered by AERONET-Caltech measurements is from 340 to 1020 nm; however, the wavelengths of the 15 H_2O absorption bands used in this study, ranging from about 1280 nm to 2200 nm, are outside the AERONET wavelength range. To calculate the AOD in these 15 bands, we use the Ångström exponent law (Seinfeld and Pandis, 2006; Zhang et al., 2015) to extrapolate the data. This law is given by:

$$\frac{\tau}{\tau_0} = \left(\frac{\lambda}{\lambda_0}\right)^{-k} \quad (2)$$

where λ and τ are the wavelength and the corresponding AOD to be interpolated, and λ_0 and τ_0 are the reference wavelength and the corresponding AOD from AERONET, and k is the Ångström exponent. k is obtained by applying linear regression using the logarithmic form of Equation (2) on the AERONET AOD measurements in the six different bands (340nm, 380nm, 440nm, 500nm, 870nm and 1020nm). A test of aerosol wavelength dependency, especially for large wavelength at 1020nm, can be found in Supplemental Material Figure 1, from which we can conclude that the wavelength dependence, which generally follows the above exponent law, is strong. The extrapolated AOD data on March 01, 2013 for the 15 bands are included in the RT model, assuming non-zero AOD is evenly distributed vertically and horizontally in the PBL.

5.1 Simulations of Daily Variation

To quantify the influence of aerosol scattering on the H_2O SCD retrievals, we simulate the bias observed by CLARS-FTS by (1) using the 2S-ESS RT model to generate synthetic spectral radiance data for the 15 chosen bands, and (2) fitting the synthetic spectral data and retrieving H_2O SCD based on Bayesian inversion theory (Rodgers, 2000) using the forward 2S-ESS RT model with the same configuration, but with AOD set to zero and held constant, as in Zhang et al. (2015). This approach approximately simulates the influence of neglecting aerosol scattering on the retrieved H_2O SCDs by CLARS. The fitting process employs the Levenberg-Marquardt algorithm (Rodgers, 2000). The state vector element to be retrieved from the inversion approach is the scaling factor, which is the ratio of retrieved H_2O SCD to the assumed "truth" data in the model from NCEP reanalysis data. We perform three experiments to demonstrate the effect of aerosol scattering on the variations in H_2O SCD retrievals. In the first experiment, denoted as Case I, the AOD data vary during the day in the same way as the AERONET-Caltech measurements, while in the second (control) experiment, denoted as Case II, the AOD data are fixed at the clear-day level, in which the lowest AOD across the year is used for all hours across the day. In the third (also control) experiment, denoted as Case III, the AOD is set to be zero for all hours across the day. The results for simulated H_2O SCD

retrieval scaling factors are shown in Figures 6(a), (b) and (c), respectively, for these three experiments. The scaling factors (f) are mean-centered by subtracting the mean to clearly show the variations in the data. The mean-centered scaling factor is calculated as: $\hat{f}_i = f_i - \bar{f}$ for i = 1 to 15, where f_i is the scaling factor, $\hat{f}_i$ is the mean-centered scaling factor for band i, and $\bar{f}$ is the mean of the scaling factors. From Figure 6(a), we can see that the variation in the simulated H_2O SCD retrievals increases with increasing AOD from the morning to the afternoon, similar to what we see from the CLARS observations in Figures 3(b) and (c). The scattering effect is stronger in the afternoon than in the morning, shown in Figure 6(b), even though the AOD is the same for all hours, probably due to the changes in SZA and AZA from the morning to the afternoon. However, since the results from the control experiment show much smaller diurnal changes, as shown in Figures 6(b) and (c), than the first experiment, aerosol scattering must be the dominant cause of the variations in H_2O SCD retrievals. Further confirmation of this is provided by Figure 6(d), which shows the comparison between CLARS measurements and the three RT model experiments in terms of normalized standard deviation of H_2O SCDs. As with the CLARS measurements, the standard deviations of the scaling factors are calculated using equation (1). To emphasize the relative change in variations of H_2O SCDs between measurements and simulations, their standard deviations (σ) are normalized to lie between 0 and 1. The normalized standard deviations are calculated as $\tilde{\sigma}_t = (\sigma_t - \sigma_{min})/(\sigma_{max} - \sigma_{min})$, where σ_t is the standard deviation, $\tilde{\sigma}_t$ is the normalized standard deviation at time t, and σ_{max} and σ_{min} are the maximum and minimum standard deviations, respectively, throughout the day. This normalization is independently implemented for measurements and simulations. When normalizing the CLARS measurements, the half-hourly means of the data are calculated to obtain the maximum and minimum. From Figure 6(d), we can see that the increasing trend from measurements is very similar to that from the simulations from the first experiment, while the trend is much smaller for the control experiment. The major difference between these results can be attributed to the effect of aerosol scattering in the PBL. Hence, we conclude that aerosol scattering is the dominant factor contributing to the variations in H_2O SCD retrievals, and the correlation between AOD and standard deviations of H_2O SCD retrievals from measurements is robust. Therefore, the H_2O SCD retrievals from CLARS can be potentially used for constraining the aerosol properties in the LA basin.

5.2 Simulations of Seasonal Variation

To investigate the sensitivity of the correlation between variations in H_2O SCDs and the corresponding AOP (as shown in Figure 4) to aerosol scattering properties, we reproduce the correlation using the 2S-ESS RT model with input AERONET AOD data, aerosol compositions (shown in Figure 5) derived from MERRA aerosol reanalysis data, and aerosol scattering properties (shown in Table 1), including SSA and g, computed by the GOCART model for the 68 days (discussed in Section 4.2) at 13:00 local time. The retrieval algorithm is the same as that described in Section 5.1. After obtaining the retrieved scaling factor for H_2O SCD for each of the 68 days, the simulated H_2O SCD retrieval is calculated as the product of the scaling factor and the H_2O abundance truth, which is set to be the mean of the H_2O SCD retrievals from the 15 bands used by the CLARS-FTS operational retrieval algorithm. The result is shown in Figure 7(a). We can see that the strong linear

correlations between the standard deviations of H_2O SCDs and the corresponding AOP are well reproduced with higher R^2 for both winter-spring and summer-autumn periods. However, the slopes from the linear regression in the simulations are slightly overestimated (by about 20%) relative to those for the CLARS data (as shown in Figure 4), probably due to the uncertainties of the input climatology aerosol compositions or single scattering properties. Interestingly, the ratio of the slope from winter-spring to that from summer-autumn periods from 2S-ESS, which is about 2.0, agrees well with that from CLARS observations. On the other hand, the difference between the two slopes become very small in Figure 7(b). This suggests that the difference in H_2O abundance between the winter-spring and summer-autumn periods is responsible for the slope difference. Similar control experiments implemented to examine the impact of variations of SSA and g are shown in Figures 7(c) and (d), respectively. We can see that the results are very similar to those in Figure 7(a), suggesting that the variations of SSA and g are not the key contributors to the variations of the standard deviations of H2O SCDs. However, the difference of slopes in Figure 7(d) are slightly smaller compared to those in Figure 7(a), indicating that g contributes to the small difference which still exists in Figure 7(b) even when the AOD does not vary. To further investigate the impact of g on the slope, Figure 7(e) shows the result from 2S-ESS with the same settings as those in Figure 7(a) but with g reduced by 50%; we can see that the slopes for the two time periods become smaller (by about 13%), indicating that the scattering effects become stronger when g is reduced. This is because, when g is smaller, the aerosol scattering phase function becomes less forward peaked and more light is scattered at scattering angles around 40 degrees, which is the scattering angle for CLARS at noon time. Small aerosols, such as organic carbon, black carbon and sulfate from urban pollution and biomass burning have much smaller SSA and g, as shown in Table 1, suggesting that the slope will also be small during events that are dominated by these small aerosols. From these results, we can conclude that the strong linear correlation between AOD and variations in H2O SCDs is robust, and that g is the main contributor to the ratio of the changes (the slope in linear regression) between them.

6 Discussion

6.1 Assumptions

When comparing the H_2O SCD retrievals from CLARS for the West Pasadena target with AOD data from AERONET-Caltech in Figures 3 and 4, two assumptions are made: (1) we assume homogeneous aerosol distribution between West Pasadena and Caltech. Since the distance between them is 5 km, which is small in terms of the whole LA basin, we expect the AOD variations at Caltech and West Pasadena to be similar. However, local topography is complex and the AOD horizontal distribution can be inhomogeneous (Lu et al., 1994). The differences between these two locations may contribute to the scatter of data and slightly lower R^2 in Figure 4(b) compared to Figure 4(a); (2) we assume, in Figure 4, that the changes in CLARS observation geometry and PBLH at noon across the days in 2013 within either winter-spring or summer-autumn are small, as well as their effects on the variations in H_2O SCD retrievals from multiple bands. This assumption is

supported by the results from RT modeling that contributions from factors other than AOD are very small even though the diurnal variations in observation geometry and PBLH are large.

6.2 Limitations

There are some limitations of the approach outlined here. First, in the 2S-ESS RT model, we use the climatological aerosol types and size distributions in LA because of the lack of temporally resolved measurements of aerosol properties in this region. In the future, more cases with different compositions of aerosol should be incorporated into the RT model to further explore this proposed approach. Second, due to the limited number of concurrent observations of H_2O SCD and AOD, the correlation is only explored in two different time periods in 2013, the winter-spring seasons and summer-autumn seasons. Correlation between the two data sets over smaller time intervals can provide more detailed information on the aerosol properties. Finally, the CLARS data are explored for the West Pasadena target only since this location is closest to the AERONET-Caltech station, which is regarded as the ground truth. Unfortunately, the Caltech campus is out of sight for the CLARS observatory near the top of Mt. Wilson. More data from other CLARS targets may be explored in the future.

7 Conclusions

We illustrate the robust ability of using multi-wavelength retrievals of water vapor slant columns to describe aerosol scattering effects. We apply this approach to H_2O SCD retrievals from 15 different absorption bands using spectral data observed by CLARS-FTS. We explore the correlation between the variation in H_2O SCDs and concurrent AOD measurements from AERONET-Caltech, and use the 2S-ESS RT model to quantitatively demonstrate the dominant role of aerosol scattering on the variation in H_2O SCD data and justify the potential of using H_2O retrievals to quantify aerosol scattering effects. We find that: (1) the wavelength dependence of aerosol scattering can be clearly observed by comparing the CLARS H_2O SCD retrievals between SVO and LABS modes; (2) a significant linear correlation is found between the standard deviations of H_2O SCDs and AOD data. Results from RT modeling are consistent with the observations, demonstrating that aerosol scattering is the dominant cause of the variation in H_2O SCDs. The ratio of AOD changes to variations in the retrieved H_2O SCD depends strongly on the asymmetry parameter of the aerosol phase function. These two pieces of evidence justify our proposed approach to derive the aerosol scattering effects using H_2O retrievals, providing a sensitive way to quantify the effect of aerosol scattering in GHG retrievals and potentially contribute towards reducing biases in GHG retrievals from space.

Acknowledgments

We thank M. Gunson and A. Eldering for stimulating discussions and support, and M. Gerstell for proofreading the manuscript. Part of the research in this study was performed at the Jet Propulsion Laboratory (JPL), California Institute of Technology (Caltech), under a contract with the National Aeronautics and Space Administration (NASA). Support from the Caltech KISS Megacity project, the NIST GHG and Climate Science Program and NASA's Carbon Cycle Science Program through the JPL is gratefully acknowledged. Z.-C. Zeng was supported by a postgraduate studentship for overseas academic exchange from the Chinese University of Hong Kong. We thank Jochen Stutz and his staff for their effort in establishing and maintaining the AERONET Caltech site. The AERONET data for this paper can be downloaded online (http://aeronet.gsfc.nasa.gov); CLARS-FTS data are available from the authors upon request.

References

Aben, I., Hasekamp, O., and Hartmann, W.: Uncertainties in the space-based measurements of CO_2 columns due to scattering in the Earth's atmosphere, J. Quant. Spectrosc. Radiat. Transfer, 104, 450–459, doi:10.1016/j.jqsrt.2006.09.013, 2007.

Bovensmann, H., Burrows, J. P., Buchwitz, M., Frerick, J., Noeel, S., Rozanov, V. V., Chance, K. V., and Goede, A. P. H.: SCIAMACHY: mission objectives and measurement modes, J. Atmos. Sci., 56, 127–150, 1999.

Buchard, V., da Silva, A. M., Colarco, P. R., Darmenov, A., Randles, C. A., Govindaraju, R., Torres, O., Campbell, J., and Spurr, R.: Using the OMI aerosol index and absorption aerosol optical depth to evaluate the NASA MERRA Aerosol Reanalysis, Atmos. Chem. Phys., 15, 5743–5760, doi:10.5194/acp-15-5743- 2015, 2015

Butz, A., Hasekamp, O. P., Frankenberg, C., and Aben, I.: Retrievals of atmospheric CO_2 from simulated space-borne measurements of backscattered near-infrared sunlight: accounting for aerosol effects, Appl. Optics, 48, 3322–3336, doi:10.1364/AO.48.003322, 2009.

Chin, M., Ginoux, P., Kinne, S., Torres, O., Holben, B. N., Duncan, B. N., Martin, R. V., Logan, J. A., Higurashi, A., and Nakajima, T.: Tropospheric aerosol optical thickness from the GOCART model and comparisons with satellite and Sun photometer measurements, J. Atmos. Sci., 59(3), 461–483, 2002.

Colarco, P., da Silva, A., Chin, M., and Diehl, T.: On- line simulations of global aerosol distributions in the NASA GEOS-4 model and comparisons to satellite and groundbased aerosol optical depth, J. Geophys. Res., 115, D14207, doi:10.1029/2009JD012820, 2010.

Conil, S., and Hall, A.: Local regimes of atmospheric variability: A case study of southern California, J. Clim., 19, 4308–4325, doi:10.1175/JCLI3837.1, 2006.

Connor, B., Boesch, H., McDuffie, J., Taylor, T., Fu, D., Frankenberg, C., O'Dell, C., Payne, V., Gunson, M., Pollock, R., Hobbs, J., Oyafuso, F., and Jiang, Y.: Quantification of Uncertainties in OCO-2 Measurements of XCO_2: Simulations and Linear Error Analysis, Atmos. Meas. Tech. Discuss., doi:10.5194/amt-2016-128, in review, 2016.

Crisp, D., Fisher, B. M., O'Dell, C., Frankenberg, C., Basilio, R., Bösch, H., Brown, L. R., Castano, R., Connor, B., Deutscher, N. M., Eldering, A., Griffith, D., Gunson, M., Kuze, A., Mandrake, L., McDuffie, J., Messerschmidt, J., Miller, C. E., Morino, I., Natraj, V., Notholt, J., O'Brien, D. M., Oyafuso, F., Polonsky, I., Robinson, J., Salawitch, R., Sherlock, V., Smyth, M., Suto, H., Taylor, T. E., Thompson, D. R., Wennberg, P. O., Wunch, D., and Yung, Y. L.: The ACOS CO_2 retrieval algorithm – Part II: Global XCO2 data characterization, Atmos. Meas. Tech., 5, 687–707, doi:10.5194/amt-5-687-2012, 2012.

Dudhia, A., Morris, P. E., and Wells, R. J.: Fast monochromatic radiative transfer calculations for limb sounding, J. Quant. Spectrosc. Radiat. Transfer, 74(6), 745–756, doi:10.1016/S0022-4073(01)00285-0, 2002.

Eck, T. F., Holben, B. N., Reid, J. S., Dubovik, O., Smirnov, A., O'Neill, N. T., Slutsker, I., and Kinne, S.: Wavelength dependence of the optical depth of biomass burning, urban, and desert dust aerosols, J. Geophys. Res., 104, 31333–31349, 1999.

Fu, D., Pongetti, T. J., Blavier, J.-F. L., Crawford, T. J., Manatt, K. S., Toon, G. C.,Wong, K.W., and Sander, S. P.: Near-infrared remote sensing of Los Angeles trace gas distributions from a mountaintop site, Atmos. Meas. Tech., 7, 713–729, doi:10.5194/amt-7-713-2014, 2014.

Goody, R. M., and Yung, Y. L.: Atmospheric Radiation: Theoretical Basis, 2nd ed., Oxford Univ. Press, Oxford, U. K., 1989.

Guerlet, S., Butz, A., Schepers, D., Basu, S., Hasekamp, O. P., Kuze, A., Yokota, T., Blavier, J.-F., Deutscher, N. M., Griffith, D. W. T., Hase, F., Kyro, E., Morino, I., Sherlock, V., Sussmann, R., Galli, A., and Aben, I.: Impact of aerosol and thin cirrus on retrieving and validating XCO_2 from GOSAT shortwave infrared measurements, J. Geophys. Res.-Atmos., 118, 4887–4905, doi:10.1002/jgrd.50332, 2013.

Holben, B. N., Eck, T. F., Slutsker, I., Tanre, D., Buis, J. P., Setzer, A., Vermote, E., Reagan, J. A., Kaufman, Y., Nakajima, T., Lavenu, F., Jankowiak, I., and Smirnov, A.: AERONET-A federated instrument network and data archive for aerosol characterization, Remote Sens. Environ., 66, 1–16, 1998.

Kalnay, E., Kanamitsu, M., Kistler, R., Collins, W., Deaven, D., Gandin, L., Iredell, M., Saha, S., White, G., Woollen, J., Zhu, Y., Chelliah, M., Ebisuzaki, W., Higgins, W., Janowiak, J., Mo, K. C., Ropelewski, C., Wang, J., Leetmaa, A., Reynolds, R., Jenne, R., and Joseph, D.: The NCEP/NCAR 40-year reanalysis project, B. Am. Meteorol. Soc., 77, 437–471, 1996.

Liu, Y., Yang, D., and Cai, Z.: A retrieval algorithm for TanSat XCO2 observation: retrieval experiments using GOSAT data, Chinese Sci. Bull., 58, 1520–1523, 2013.

Lu, R. and Turco, R. P.: Air pollutant transport in a coastal environment. Part I. Two-dimensional simulations of sea-breeze and mountain effects, J. Atmos. Sci., 51, 2285–2308, 1994.

Newman, S., Jeong, S., Fischer, M. L., Xu, X., Haman, C. L., Lefer, B., Alvarez, S., Rappenglueck, B., Kort, E. A., Andrews, A. E., Peischl, J., Gurney, K. R., Miller, C. E., and Yung, Y. L.: Diurnal tracking of anthropogenic CO_2 emissions in the Los Angeles basin megacity during spring 2010, Atmos. Chem. Phys., 13, 4359–4372, doi:10.5194/acp-13-4359-2013, 2013.

O'Dell, C. W., Connor, B., Bösch, H., O'Brien, D., Frankenberg, C., Castano, R., Christi, M., Crisp, D., Eldering, A., Fisher, B., Gunson, M., McDuffie, J., Miller, C. E., Natraj, V., Oyafuso, F., Polonsky, I., Smyth, M., Taylor, T., Toon, G. C.,Wennberg, P. O., and Wunch, D.: The ACOS CO_2 retrieval algorithm – Part 1: Description and validation against synthetic observations, Atmos. Meas. Tech., 5, 99–121, doi:10.5194/amt-5-99-2012, 2012.

Rienecker, M. M., Suarez, M. J., Gelaro, R., Todling, R., Bacmeister, J., Liu, R., Bosilovich, M. G., Schubert, S. D., Takacs, L., Kim, G-K, Bloom, S., Chen, J., Collins, D., Conaty, A., da Silva, A., Gu, W., Joiner, J., Koster, R. D., Lucchesi, R., Molod, A., Owens, T., Pawson, S., Pegion, P., Redder, C. R., Reichle, R., Robertson, F. R., Ruddick, A. G., Sienkiewicz, M., and Woollen, J.: MERRA: NASA's Modern-Era Retrospective Analysis for Research and Applications, J. Climate, 24, 3624–3648, 2011.

Rodgers, C. D.: Inverse Methods for Atmospheric Sounding: Theory and Practice, World Scientific, Singapore, 2000.

Rothman, L. S., Gordon, I. E., Barbe, A., Benner, D. C., Bernath, P. E., Birk, M., Boudon, V., Brown, L. R., Campargue, A., Champion, J. P., Chance, K., Coudert, L. H., Dana, V., Devi, V. M., Fally, S., Flaud, J. M., Gamache, R. R., Goldman, A., Jacquemart, D., Kleiner, I., Lacome, N., Lafferty, W. J., Mandin, J. Y., Massie, S. T., Mikhailenko, S. N., Miller, C. E., Moazzen-Ahmadi, N., Naumenko, O. V., Nikitin, A. V., Orphal, J., Perevalov, V. I., Perrin, A., Predoi-Cross, A., Rinsland, C. P., Rotger, M., Simeckova, M., Smith, M. A. H., Sung, K., Tashkun, S. A., Tennyson, J., Toth, R. A., Vandaele, A. C., and Vander Auwera, J.: The HITRAN 2008 molecular spectroscopic database, J. Quant. Spectrosc. Radiat. Transfer, 110, 533–572, doi:10.1016/j.jqsrt.2009.02.013, 2009.

Seinfeld, J. and Pandis, S.: Atmospheric chemistry and physics: from air pollution to climate change, Wiley, Inc., New Jersey, USA, p.1224, 2006.

Spurr, R., and Natraj, V.: A linearized two-stream radiative transfer code for fast approximation of multiple-scatter fields, J. Quant. Spectrosc. Radiat. Transfer, 112(16), 2630–2637, doi:10.1016/j.jqsrt.2011.06.014, 2011.

Su, Z., Xi, X., Natraj, V., Li, K.-F., Shia, R.-L., Miller, C. E., and Yung, Y. L.: Information-rich spectral channels for simulated retrievals of partial column-averaged methane, Earth Space Sci., 3, 2-14, doi:10.1002/2015EA000120, 2016.

Thompson, J.E., Hayes, P.L., Jimenez, J.L., Adachi, K., Zhang, X., Liu, J., Weber, R.J. and Buseck, P.R.: Aerosol optical properties at Pasadena, CA during CalNex 2010, Atmos. Environ., 55, pp.190-200, doi:10.1016/j.atmosenv.2012.03.011, 2012.

Toon, G. C., Farmer, C. B., Schaper, P. W., Lowes, L. L., and Norton, R. H.: Composition measurements of the 1989 Arctic winter stratosphere by airborne infrared solar absorption spectroscopy, J. Geophys. Res., 97, 7939–7961, 1992.

Winker, D. M., Vaughan, M. A., Omar, A. H., Hu, Y., Powell, K. A., Liu, Z., Hunt, W. H., and Young, S. A.: Overview of the CALIPSO Mission and CALIOP Data Processing Algorithms, J. Atmos. Oceanic Technol., 26, 2310–2323, 2009

Wong, K. W., Fu, D., Pongetti, T. J., Newman, S., Kort, E. A., Duren, R., Hsu, Y.-K., Miller, C. E., Yung, Y. L., and Sander, S. P.: Mapping CH_4 : CO_2 ratios in Los Angeles with CLARS-FTS from Mount Wilson, California, Atmos. Chem. Phys., 15, 241–252, 2015.

Wong, K. W., Pongetti, T. J., Oda, T., Rao, P., Gurney, Kevin. R., Newman, S., Duren, R. M., Miller, C. E., Yung, Y. L., and Sander, S. P.: Monthly trends of methane emissions in Los Angeles from 2011 to 2015 inferred by CLARS-FTS observations, Atmos. Chem. Phys. Discuss., doi:10.5194/acp-2016-232, in review, 2016.

Wunch, D., Toon, G. C., Blavier, J.-F. L., Washenfelder, R., Notholt, J., Connor, B. J., Griffith, D. W. T., Sherlock, V., and Wennberg, P. O.: The Total Carbon Column Observing Network, Phil. Trans. R. Soc. A, 369, 2087–2112, doi:10.1098/rsta.2010.0240, 2011.

Xi, X., Natraj, V., Shia, R. L., Luo, M., Zhang, Q., Newman, S., Sander, S. P., and Yung, Y. L.: Simulated retrievals for the remote sensing of CO_2, CH_4, CO, and H_2O from geostationary orbit, Atmos. Meas. Tech., 8, 4817-4830, doi:10.5194/amt-8-4817-2015, 2015.

Yoshida, Y., Ota, Y., Eguchi, N., Kikuchi, N., Nobuta, K., Tran, H., Morino, I., and Yokota, T.: Retrieval algorithm for CO_2 and CH_4 column abundances from short-wavelength infrared spectral observations by the Greenhouse gases observing

satellite, Atmos. Meas. Tech., 4, 717–734, doi:10.5194/amt-4-717-2011, 2011.

Zhang, Q., Natraj, V., Li, K.-F., Shia, R.-L., Fu, D., Pongetti, T. J., Sander, S. P., Roehl, C. M., and Yung, Y. L.: Accounting for aerosol scattering in the CLARS retrieval of column averaged CO_2 mixing ratios, J. Geophys. Res. Atmos., 120, doi:10.1002/2015JD023499, 2015.

Zhang, Q., Shia, R.-L., Sander, S. P., and Yung, Y. L.: XCO_2 retrieval error over deserts near critical surface albedo, Earth Space Sci., 2, doi:10.1002/2015EA000143, 2016.

Table 1. Aerosol single scattering properties, computed using the GOCART model[a], for the 5 types of aerosols (black carbon, organic carbon, sulfate, dust and sea salt). Single Scattering Albedo (SSA) and asymmetry parameter (g) are averaged values over the 15 H_2O absorption bands.

	black carbon	organic carbon	sulfate	dust	sea salt
SSA	0.03	0.77	0.97	0.94	0.99
g	0.10	0.25	0.35	0.71	0.80

[a]Colarco et al. (2010) and Chin et al. (2002)

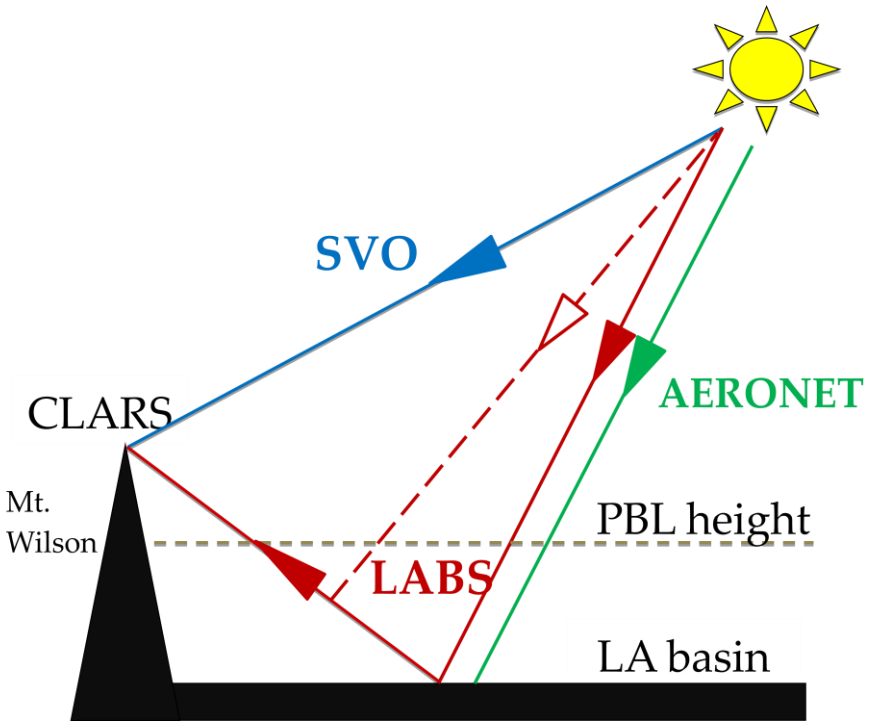

Figure 1. Schematic diagram of CLARS-FTS measurement geometries for West Pasadena and the AERONET site at Caltech. CLARS-FTS has two modes of operation, including Los Angeles Basin Survey mode (LABS; in solid red) and the Spectralon Viewing Observation mode (SVO; in blue). An example of light path change due to aerosol scattering along the path from the basin to the mountain top is illustrated (in dotted red). Also shown is the light path of AERONET-Caltech (in green).

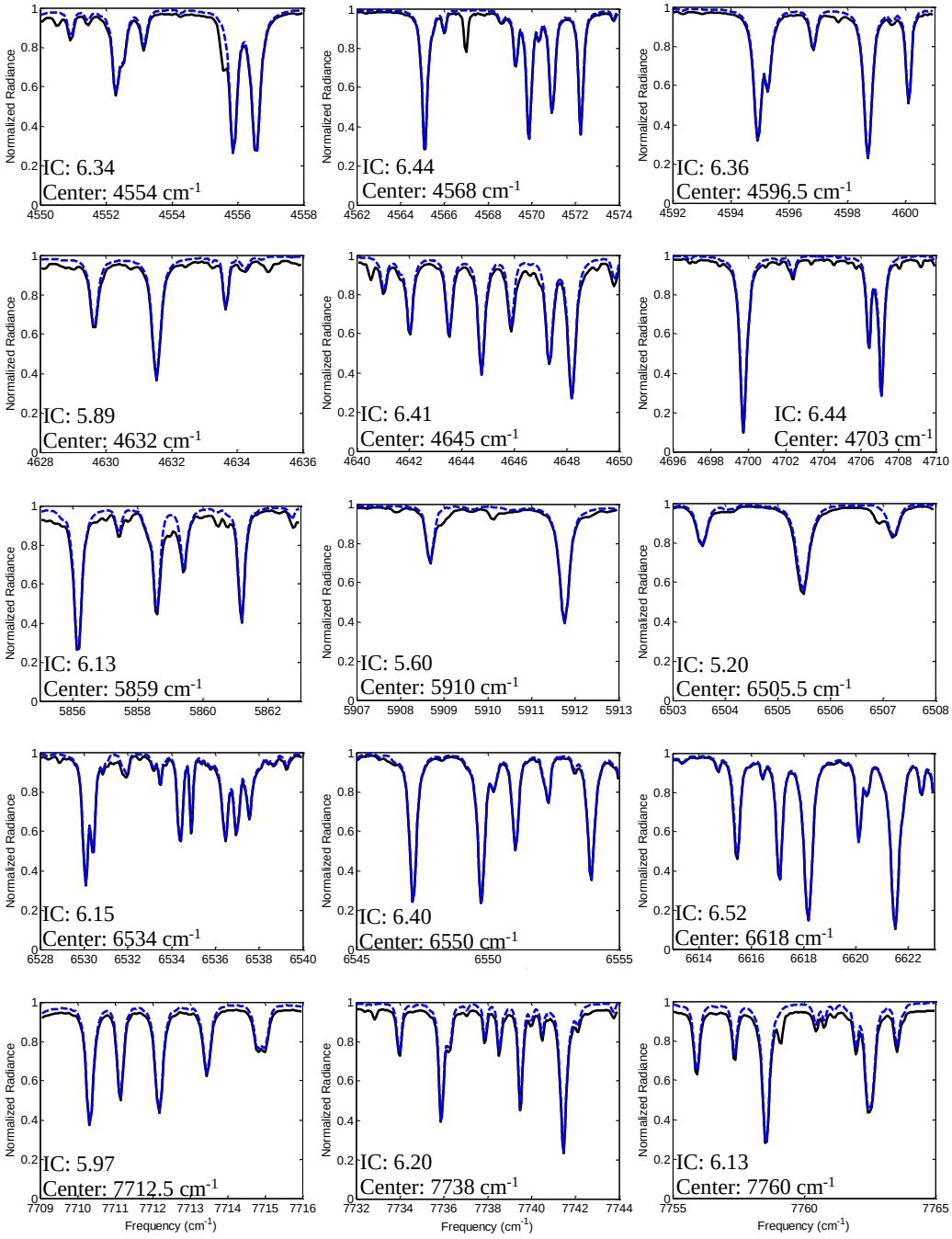

Figure 2. The normalized radiances of the 15 H_2O absorption bands selected for retrieving H_2O SCDs from CLARS-FTS measurements. These radiances are spectral fits using the CLARS-FTS measurements in West Pasadena on March 01, 2013 with a solar zenith angle (SZA) of 41.45°. Solid black curves are fits to the spectra, including contributions of all trace gases and solar lines, from spectral measurements by the FTS and dashed blue curves are the estimated contribution of H_2O absorption to the spectral fits. Contributions of other species in these spectral regions are not shown. Central wavelength and information content (IC) value of each band used for retrieving H_2O content are also indicated.

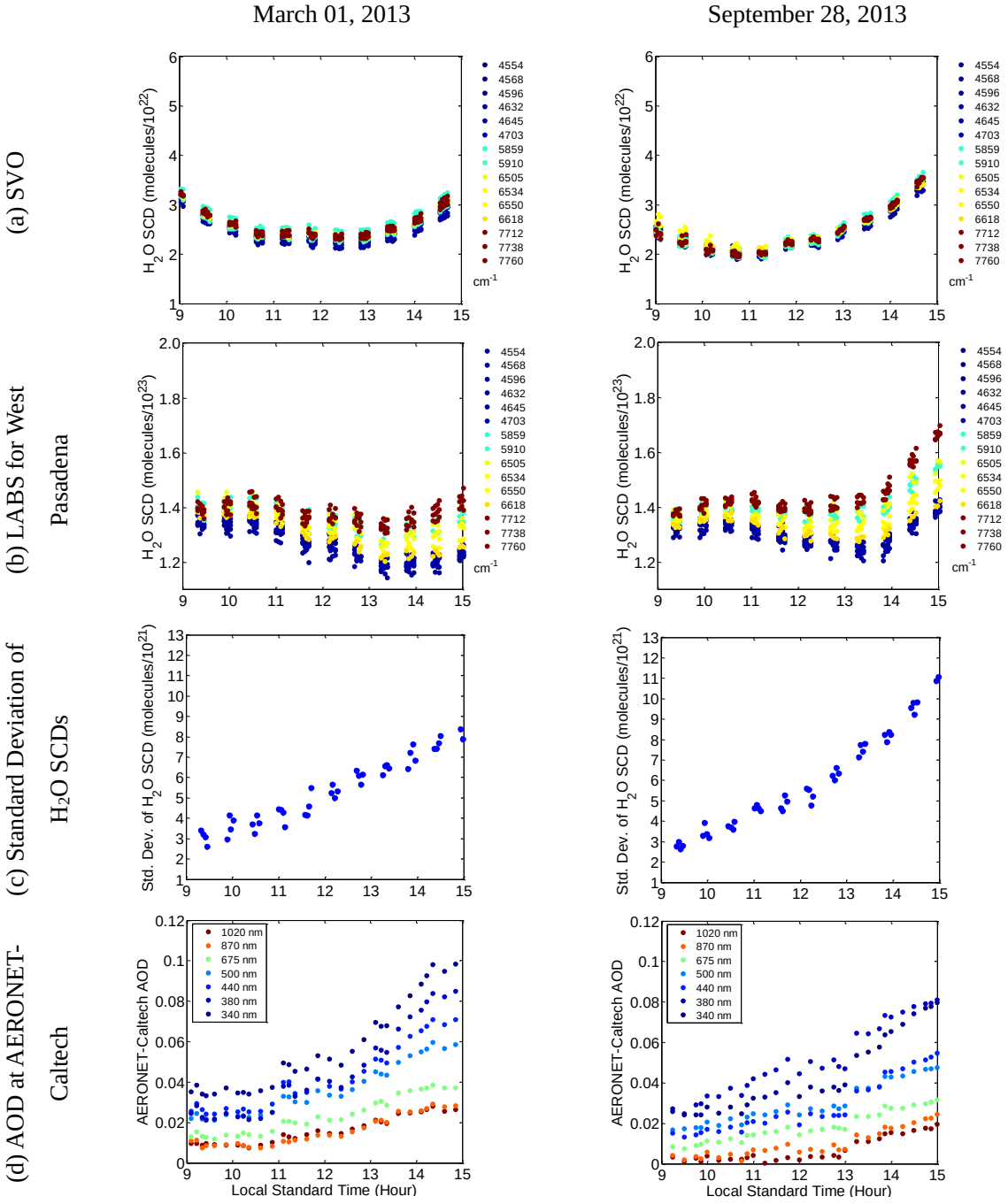

Figure 3. Daily Variations of CLARS H_2O SCD retrievals for the West Pasadena target and AOD measurements from AERONET-Caltech station on March 01, 2013 (left column) and September 28, 2013 (right column). H_2O SCD retrievals from SVO mode are shown in panel (a), and from LABS mode for West Pasadena are shown in panel (b). The corresponding standard deviations of H_2O SCD retrievals, a measure of the degree of variation in the retrievals, are shown in panel (c) and the AOD measurements from AERONET-Caltech are shown in panel (d).

(a) winter-spring

(b) summer-autumn

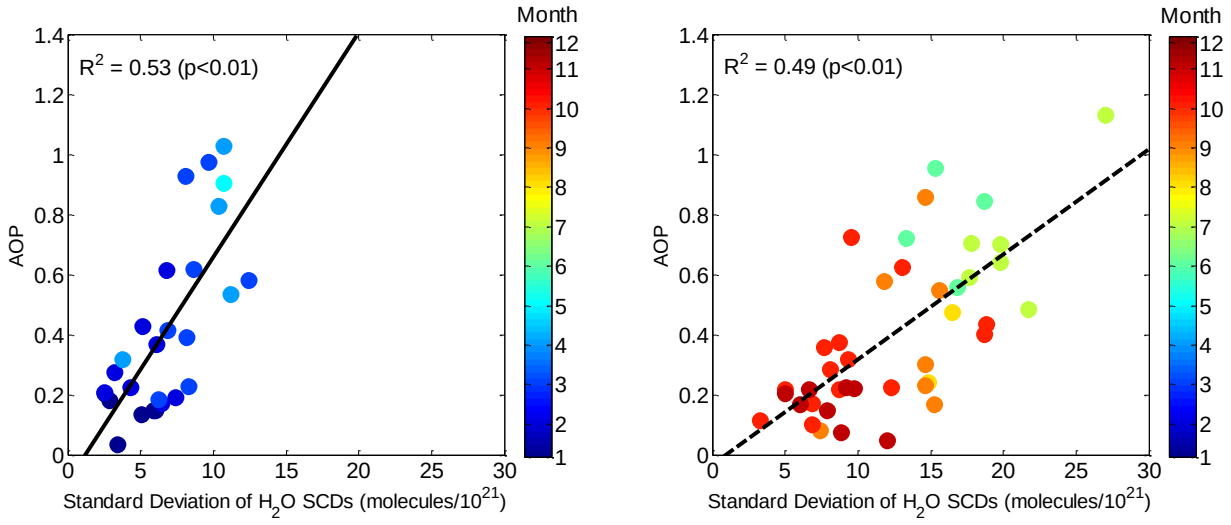

Figure 4. Correlation between daily averaged standard deviation of H_2O SCDs, a measure of retrieval differences, from 12:00 to 14:00 and the corresponding averaged AOP, calculated by scaling AOD data (1020 nm) from AERONET based on CLARS geometry, for two time periods in 2013. (a) Winter and spring, including January to May, in which the coefficient of determination (R^2) is 0.53 and [slope, intercept] = [0.08±0.03, -0.09±0.21] with 95% confidence bounds from linear regression. No December data from AERONET are available in 2013. (b) Summer and autumn from June to November, in which R^2 is 0.49 and [slope, intercept] = [0.04±0.01, -0.03±0.16]. In total, there are 68 days of daily mean data available in 2013, in which 27 days are for winter-spring and 40 days are for summer-autumn.

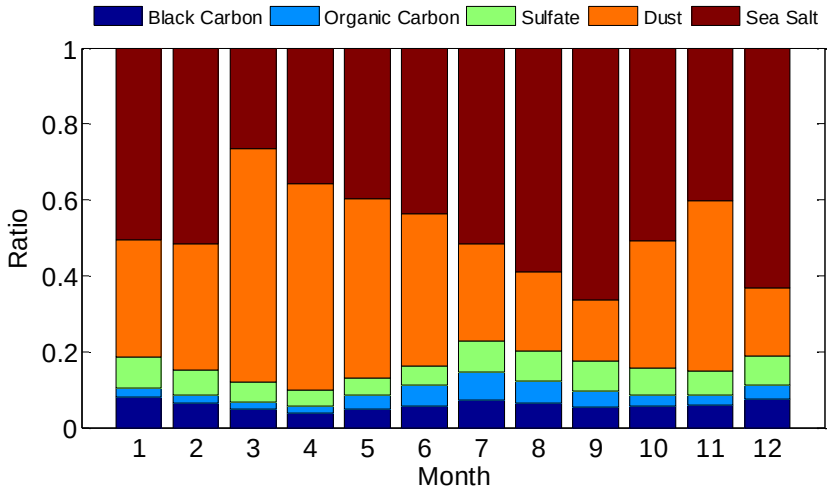

Figure 5. Monthly-averaged climatological aerosol composition (as percentages of total optical depth averaged over the 15 H_2O absorption bands) for the 5 composite MERRA aerosols (black carbon, organic carbon, sulfate, dust and sea salt) in the day time (local times 10:00, 13:00 and 16:00).

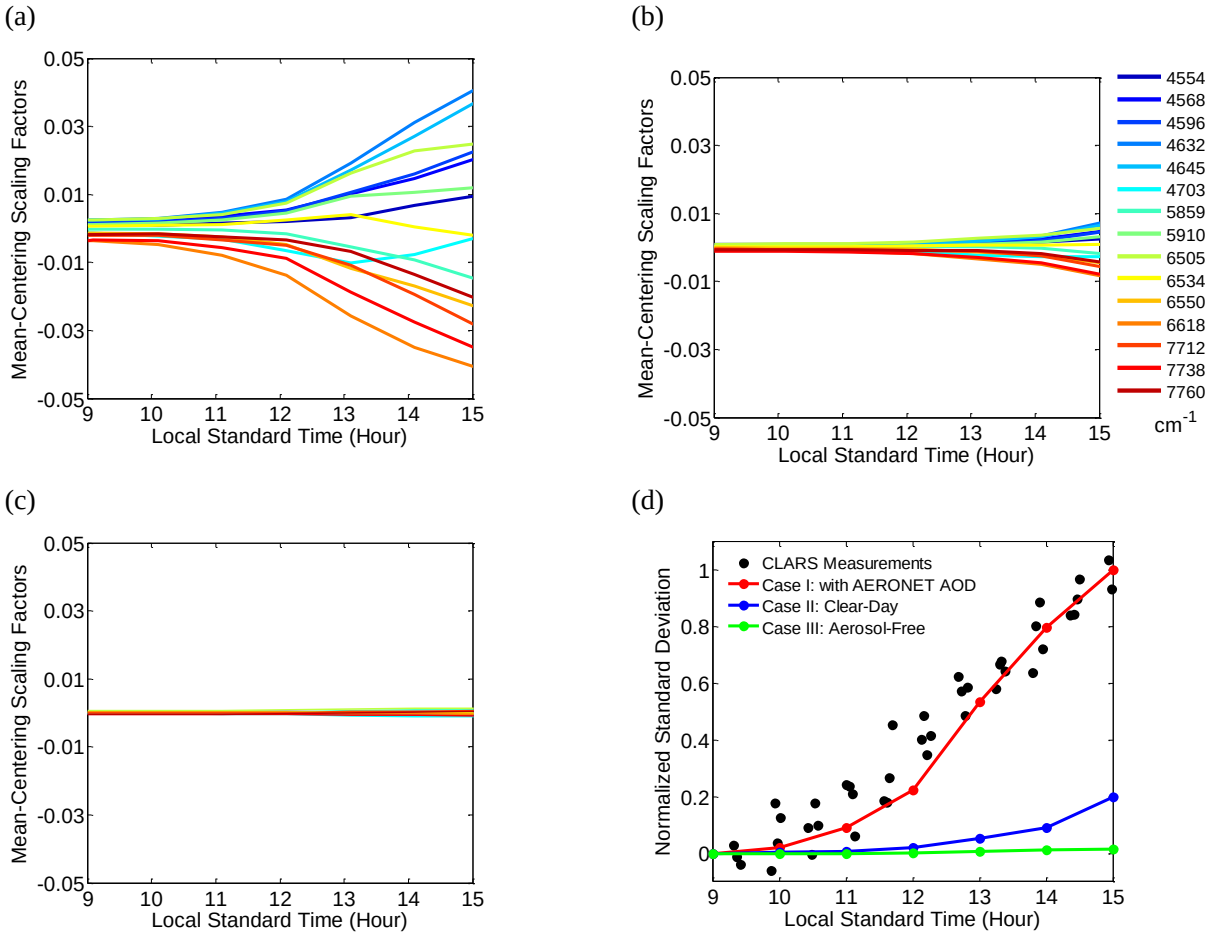

Figure 6. (a) Case I: scaling factors for H_2O SCDs retrieved from the simulated synthetic spectral radiance of the 15 chosen bands using 2S-ESS RT model with AOD data from AERONET-Caltech on March 01, 2013. The scaling factors are mean-centered by subtracting the mean to clearly show the variations in the retrievals; (b) Case II: same as (a) except that the AOD is fixed at the clear-day level, in which the lowest AOD in 2013 is used for all hours across the day; (c) Case III: same as (a) except that the AOD is set to be zero for all hours across the day; (d) Comparison between CLARS measurements and results from the three RT model experiments in (a), (b) and (c) in terms of standard deviations, a measure of variations in H_2O SCDs retrieved from the 15 chosen bands. The standard deviations are normalized to be between 0 and 1 for both measurements and simulations. The half-hourly mean of the CLARS data is calculated to obtain the maximum and minimum for the normalization.

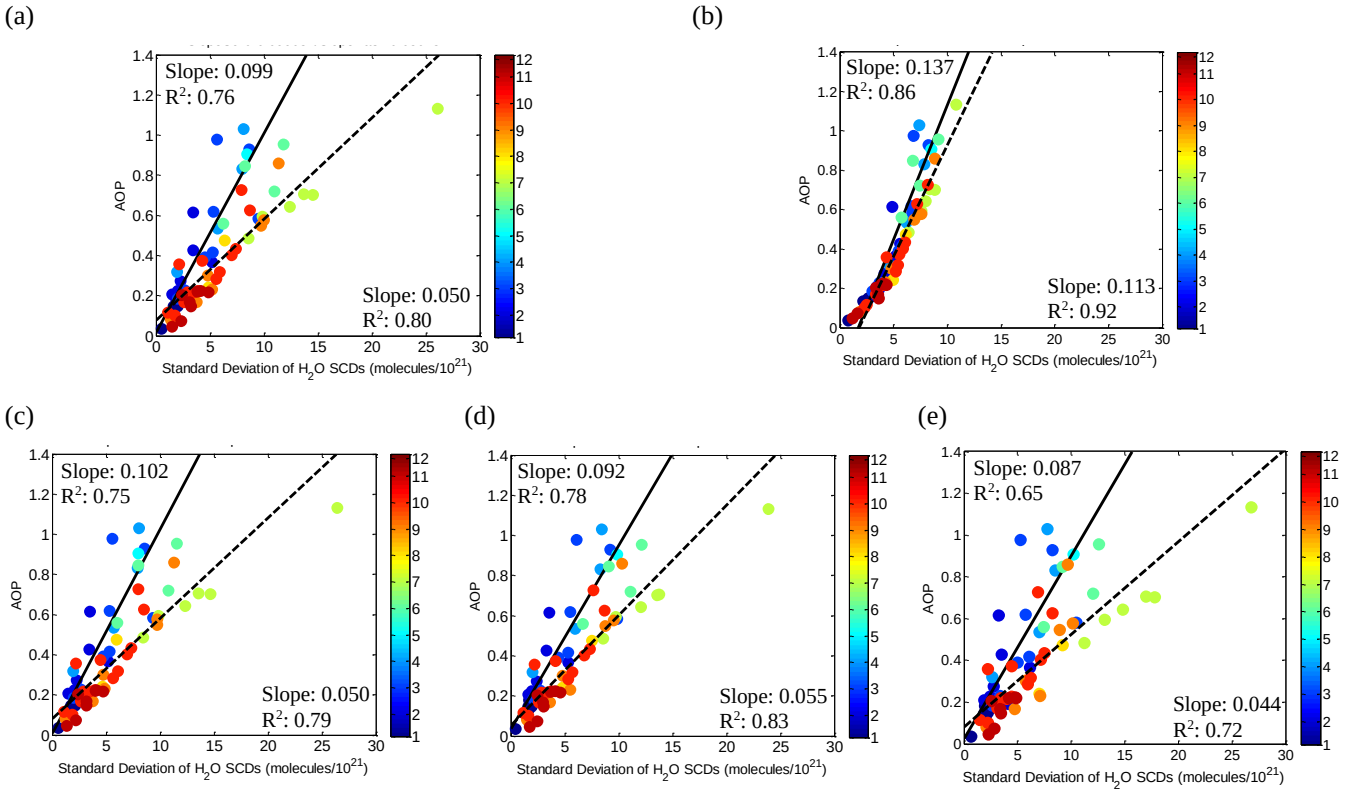

Figure 7. Reproduction of the correlation, as shown in Figure 4, between daily averaged standard deviation of H_2O SCDs at noon and the corresponding averaged AOP for two time periods in 2013, using the 2S-ESS RT model. The input AOD data are obtained from AERONET, aerosol compositions are derived from MERRA aerosol reanalysis data, and the related scattering properties, including single scattering albedo (SSA) and asymmetry parameter (g), are computed using the GOCART model. The slopes and R^2 from the linear regression of winter-spring period (solid line) and summer-autumn period (dash line) are shown on the upper-left and bottom-right corners, respectively. Results from five experiments are presented, including (a) the linear correlation reproduced by 2S-ESS with averaged AOD data between 12:00 and 14:00 and compositions for 5 composite aerosols (black carbon, organic carbon, sulfate, dust, and sea salt) at 13:00 for the 68 days; (b) same as (a) except that the H_2O SCD truth is fixed for all days at the mean value for the 68 days in 2013, in order to examine the impact from variability in H_2O abundance; (c) same as (a) except that the SSA is fixed for all days at the mean value for the 68 days in 2013, in order to examine the impact from SSA variations; (d) same as (a) except that g is fixed for all days at the mean value for the 68 days in 2013, in order to examine the impact from g variations; (e) same as (a) except that g for each of the 68 days is set at half of the original value, in order to examine its contribution to the linear correlation.

Supplement of

Aerosol Scattering Effects on Water Vapor Retrievals over the Los Angeles Basin

Zhao-Cheng Zeng et al.

Correspondence to: zcz@gps.caltech.edu

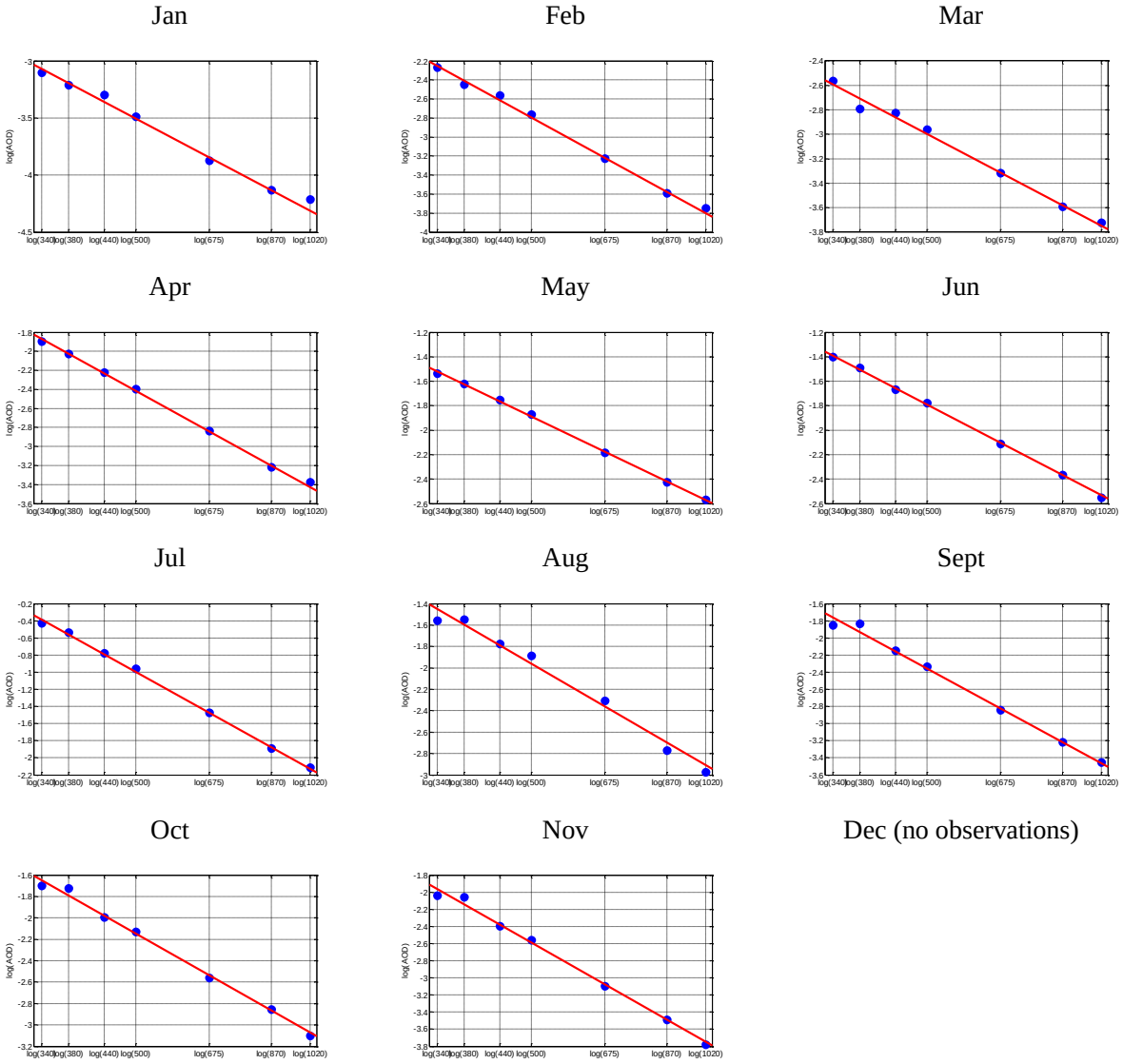

Supplemental Material Figure 1. Examples from applying linear regressions using the logarithmic form of Ångström exponent law on the AERONET AOD data at noon time around 13:00, for the 11 different months, selected from the 68 days of data shown in Figure 4 and 7. The blue dots are the AERONET AOD measurements in the seven different bands (340nm, 380nm, 440nm, 500nm, 870nm and 1020nm) and the red line is linear regression result from the first 6 of the 7 bands (that is, 1020nm is excluded). Therefore, the closeness of the AOD at 1020nm to the fitted red line indicates the strength of the wavelength dependence that follows the exponential law. The averaged bias between the AOD and the red line value at 1020nm for all the 68 days is 9.82±10.02% (mean and one standard deviation).